Heats of Formation of *t*-Butyl Peroxy Radical and *t*-Butyl Diazyl Ion: RRKM vs SSACM Rate Theories in Systems with Kinetic and Competitive Shifts

Nicholas S. Shuman,[†,‡] Andras Bodi,[§] and Tomas Baer*[,†]

Department of Chemistry, The University of North Carolina, Chapel Hill, North Carolina 27599 and Swiss Light Source, Paul Scherrer Institut, 5232 Villigen, Switzerland

Received: August 11, 2009; Revised Manuscript Received: September 30, 2009

The dissociations of energy-selected di-*t*-butyl peroxide and di-*t*-butyl diazene ions have been studied by threshold photoelectron−photoion coincidence (TPEPICO) spectroscopy. Di-*t*-butyl peroxide ions dissociate via two parallel channels: (1) methyl loss at a 0 K onset (E_0) of 9.58 ± 0.04 eV followed by a sequential dissociation of the daughter ion to produce $C_4H_9O^+$ and acetone; and (2) the dominant dissociation channel, producing *t*-butyl ion and *t*-butyl peroxy radical at an E_0 of 9.758 ± 0.020 eV. Di-*t*-butyl diazene ions dissociate through three parallel channels: (1) a rearrangement to form isobutene ion; (2) C−N bond cleavage with the charge staying on the *t*-butyl diazyl species (E_0 = 8.069 ± 0.050 eV); and (3) C−N bond cleavage with the charge instead on the *t*-butyl (E_0 = 8.122 ± 0.050 eV); the coproduct for this latter channel is a weakly, or possibly unbound, $N_2\cdots$*t*-butyl structure. Both the peroxide and diazene ion dissociations produce metastable daughters, and the dissociation rates are modeled with two rate theories: the Rice−Ramsperger−Kassel−Marcus (RRKM) theory and a simplified version of the statistical adiabatic channel model (SSACM). Due to a large kinetic shift, RRKM incorrectly models the peroxide ion rate curve. Using SSACM, the heat of formation of *t*-butyl peroxy radical is determined to be ΔH°_{0K} = − 81.1 ± 3.9 kJ mol^{-1}, and, using B3LYP/6-311++G(d,p) thermal energy, ΔH°_{298K} = − 109.7 ± 3.9 kJ mol^{-1}. Due to a competitive shift of the higher energy channel onsets, RRKM also incorrectly models the diazene rate curves. The 298 K heat of formation of the *t*-butyl diazyl ion, which is bound by 14 kJ mol^{-1}, is determined to be 701.2 ± 5.9 kJ mol^{-1}.

Introduction

Alkyl peroxy radicals are key intermediates in both combustion processes and in the atmospheric oxidation of organic compounds and may play an important role in a range of pathological processes.[1,2] Accurate thermochemical values are important in the understanding of these systems. However, because peroxy radicals are fairly reactive intermediates with fleeting lifetimes, experimental observation of their properties is challenging. In particular, few experimental alkyl peroxy radical enthalpies of formation have been reported, and even those have relatively large uncertainties on the order of 5−10 kJ mol^{-1}.[3,4] Theoretical studies of alkyl peroxy radical thermochemistry are more numerous;[5–9] however, comparison to experimental values is needed to confirm or refute the accuracy of calculations on these open shell compounds.

The thermochemistry of alkyl diazyl radicals (the nitrogen analogues to peroxy species) is also poorly known. Despite a lengthy history of mechanistic and kinetics studies on alkyl diazyl dissociation,[10] only a handful of alkyl diazyl radical[11,12] and no alkyl diazyl ion heats of formation have been reported. In particular, there has been debate spanning eight decades[13,14] over whether or not alkyl diazyl radicals are formed as intermediates in the decomposition of various alkyl diazenes to alkyl radicals and N_2.

Threshold photoelectron−photoion coincidence (TPEPICO) spectroscopy is, in general, an attractive experimental route to radical heats of formation. TPEPICO determines the 0 K onset (E_0) of a neutral molecule dissociating to a fragment ion, a fragment radical, and an electron. If the heat of formation of both the parent molecule and the daughter ion are well-known, then the heat of formation of the radical is determined by

$$\Delta H^\circ_{f,0K}[\text{radical}] = E_0 + \Delta H^\circ_{f,0K}[\text{molecule}] - \Delta H^\circ_{f,0K}[\text{ion}] \quad (1)$$

TPEPICO of alkyl peroxide compounds should give access to the thermochemistry of alkyl peroxy radicals because, unlike peroxide neutrals that decompose by O−O bond cleavage, the weakest bond in alkyl peroxide radical ions is typically the C−O bond.[3] Unfortunately, many alkyl peroxide compounds tend to be difficult to investigate as the neutrals readily dissociate in the gas phase. A notable exception is di-*t*-butyl peroxide, $(CH_3)_3COOC(CH_3)_3$, which has previously been observed to dissociate upon electron impact to the *t*-butyl ion and *t*-butyl peroxy radical.[15] An accurate determination of E_0 for this channel allows for the derivation of the enthalpy of formation of the *t*-butyl peroxy radical.

Mayer et al.[16] have recently shown that di-*t*-butyl diazene ions (the nitrogen analogue of di-*t*-butyl peroxide) similarly fragment primarily to produce the *t*-butyl ion (m/z = 57) and the *t*-$C_4H_9NN^+$ (m/z = 85) as a minor product. Because the heat of formation of the diazene neutral and *t*-butyl radical[17] and ion[18] are well established, the measured E_0 values for this system (7.83 eV for m/z = 85 and 7.94 eV for m/z = 57) would yield both the *t*-butyl diazyl radical and *t*-butyl diazyl ion heats of formation. However, inspection of the Mayer et al. TPEPICO

* To whom correspondence should be addressed.
† The University of North Carolina.
‡ Current address: Air Force Research Laboratory, Space Vehicles Directorate, 29 Randolph Road, Hanscom Air Force Base, Massachusetts 01731-3010.
§ Paul Scherrer Institut.

10.1021/jp907767c
Published on Web 11/11/2009

results for both of these channels suggests that the dissociation rates were modeled incorrectly and the reported onsets are too low.

There exists a long-standing issue in modeling the dissociation rates of large ions with many low energy modes such as those investigated here. Often these dissociations occur with minimum rates too slow to be measured directly on the microsecond time scale typical for mass spectrometry experiments, resulting in a kinetic shift[19] between the thermochemical and observed dissociation onsets; product ions may not be detected several hundred millielectronvolts to several electronvolts above the dissociation threshold. In order to determine E_0 correctly, the dissociation rate curve must be extrapolated to low ion internal energies from rates measured directly at higher energies. The dissociations are often barrierless (indeed, extracting thermochemical values from measured onsets requires the absence of a reverse barrier) and lack a well-defined transition state, which is contrary to an assumption of the rigid-activated complex Rice−Ramsperger−Kassel−Marcus (RRKM) theory.[20] Despite this, RRKM still correctly describes the rate curves of a barrierless ionic dissociation in at least one instance (that of iodobenzene ion),[21] and its simplicity makes it an attractive alternative to the more appropriate but arduous methods, variational transition state theory (VTST)[22–24] or the statistical adiabatic channel model (SACM)[25] combined with classical trajectory calculations. The difficulty lies in identifying when RRKM will fail to describe the rate curve, and a more rigorous method must be applied. Troe and co-workers have recently shown that this issue can be side-stepped by employing a simplified version of SACM (SSACM),[26] requiring no more input or calculation than RRKM.[21,27] Here we analyze the dissociations of di-*t*-butyl peroxide ions, which occur with a large kinetic shift, and di-*t*-butyl diazene ions, which occur with almost no kinetic shift, by both RRKM and SSACM and compare the thermochemical values derived using the different rate theories.

Experimental Methods

Two different threshold photoelectron photoion coincidence setups were used. The di-*t*-butyl peroxide data were obtained on the TPEPICO apparatus in Chapel Hill, which has previously been described in detail.[28–30] The di-*t*-butyl diazene was investigated using the imaging PEPICO (iPEPICO) experiment[31] at the vacuum ultraviolet (VUV) beamline of the Swiss Light Source (SLS) in Villigen, Switzerland.[32] A number of points were repeated in Chapel Hill in order to verify reproducibility of the results. In both set-ups, sample vapor (di-*t*-butyl peroxide and di-*t*-butyl diazene, obtained from Sigma-Aldrich and used without further purification) is introduced to a high-vacuum chamber, ionized by continuously tunable VUV radiation, and threshold (zero-kinetic energy) electrons, and their corresponding ions are detected in coincidence to produce time-of-flight (TOF) mass spectra of energy-selected ions.

In the Chapel Hill experiment, sample vapor passes through several inches of copper tubing and a stainless steel needle held at a constant temperature (di-*t*-butyl peroxide: 255 ± 1 K; di-*t*-butyl diazene: 295 K). Previous experiments suggest that the transit time is sufficient for the sample to reach thermal equilibrium.[29] Molecules are ionized by VUV light from a hydrogen discharge lamp dispersed by a 1 m focal length monochromator providing a resolution of 8 meV (~1 Å) at 10 eV. Photoions and photoelectrons are accelerated in opposite directions by a constant 20 V cm^{-1} field. Electrons are focused by velocity focusing electron optics so that those with zero velocity transverse to the axis of propagation (including both threshold electrons and excited electrons with a velocity vector that points directly along the axis of propagation) are detected by a Channeltron electron multiplier masked by a 1 mm aperture. A second Channeltron detector sits off-axis masked by a rectangular 2 mm × 5 mm aperture and collects a representative portion of electrons with nonzero kinetic energy to be used in a scheme to correct data for hot-electron contamination.[28] Ions are accelerated in two stages to ensure space focusing, followed by a 26 cm drift region, and a deceleration voltage and second 5 cm drift region in order to separate stable parent ions from fragment ions born in the first drift region. Ions are detected by tandem microchannel plates. Each detected electron provides a start signal to a time-to-pulse-height converter, and the subsequently detected ion provides a stop signal. The output pulses are collected by multichannel analyzer boards to produce two TOF mass spectra, one each for electrons detected by the on-axis "center" Channeltron or the off-axis Channeltron. Subtraction of the latter spectrum from the corresponding center spectrum results in an energy-selected TOF spectrum, so that the internal energy of each parent ion is defined by the sum of the photon energy and the ion's initial thermal energy less the adiabatic ionization energy.

The iPEPICO experiment at the SLS uses dispersed light from the X04DB bending magnet beamline as the source of VUV radiation.[31] The other major difference between it and the Chapel Hill set up is that the electron and ion extraction field is 80 V cm^{-1}, and the velocity-focused electrons are collected on a Roentdek DLD40 imaging detector, which provides a combined electron and photon resolution of 2 meV. Finally, instead of a single start−single stop coincidence scheme with time-to-pulse-height converters, the iPEPICO data acquisition operates in the multistart−multistop mode, and can thus accommodate the much higher acquisition rates resulting from the 3 orders of magnitude higher photon flux (10^{11} vs 10^8 s^{-1} in the Chapel Hill setup).[33] Hot electron subtraction is accomplished by using the coincidence counts associated with user-defined regions of the imaging plate.

In both experiments, peak shapes and arrival times in the TOF spectra are functions of not just the mass, but also the dissociation time of the ions. Parent ions that do not dissociate during the TOF appear as a sharp peak with a characteristic shape representing the initial velocity distribution of molecules in the ionization region. Fragment ions that dissociate within about 10^{-7} s of ionization appear at a TOF characteristic of the fragment mass. Ions that dissociate at a slightly longer time have already traveled noticeably along the propagation axis and as a result appear at a slightly longer TOF, resulting in an asymmetric fragment ion peak shape reflecting the rate of the dissociation of the parent ion. Ions that dissociate while in the first drift region are left with less kinetic energy than those formed immediately after ionization and are therefore decelerated more than parent ions, causing these fragments to appear at a longer TOF than the parent ion peak.

Analysis of the data by SSACM or RRKM requires the density of states of the dissociating ion as well as the number of states of products ions and neutrals and transition states. These are calculated by the Beyer−Swinehart direct count method[20] using harmonic vibrational frequencies and rotational constants calculated with Gaussian 03 quantum chemical software.[34] Geometries for reactant and product molecules and ions are optimized and unscaled[35] frequencies determined using the B3LYP functional with the 6-311++G(d,p) basis set. The simple bond cleavage channels are assumed to be barrierless,

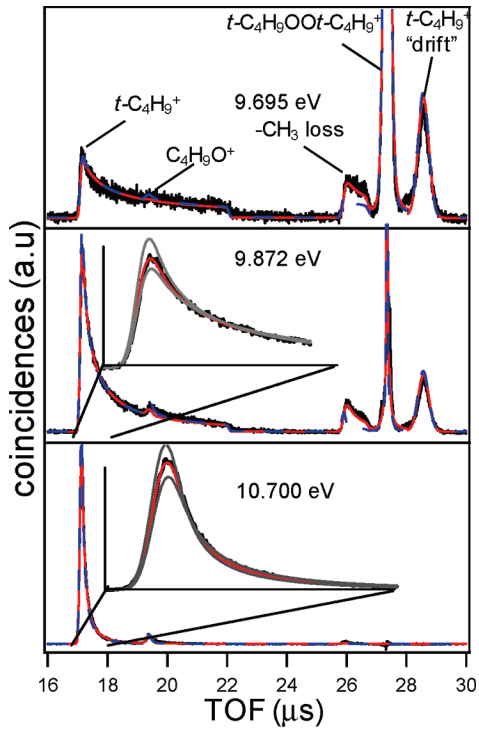

Figure 1. TPEPICO TOF distributions for di-*t*-butyl peroxide. Experimental (black lines) and best-fit simulated SSACM (red lines, see text) and RRKM (dashed blue lines) TOF spectra at the indicated photon energies. The degree of asymmetry of the metastable daughter ion peaks is indicative of the dissociation rate. Insets show an expanded view of the *t*-butyl daughter ion along with SSACM simulated fits at the high and low uncertainty limits of the onset to channel 3 (gray lines).

lacking a transition state at an energetic maximum. Instead, transition state structures and frequencies used in the RRKM rate analysis are determined by a constrained optimization of the dissociating ion with the breaking bond stretched to about 4 Å. The five lowest frequencies of the resulting structure are the transitional modes decaying from vibrations into orbital motions of the products and are treated as optimizable parameters in the RRKM analysis.

Results and Analysis

I. Di-*t*-butyl Peroxide. Representative TOF spectra of di-*t*-butyl peroxide at several photon energies are shown in Figure 1. The relative abundances of the parent and daughter ions as a function of photon energy (i.e., the breakdown diagram) appear in Figure 2. The solid lines through the data points are a result of our modeling that takes into account the initial thermal energy of the sample and the slow dissociation of the parent ions. It is evident that two channels compete at low ion internal energies, with C−O bond cleavage dominating the product branching over methyl-loss. At higher energies, a small abundance of $C_4H_9O^+$ product appears. It is tempting to assume the $C_4H_9O^+$ ion results from a simple O−O bond cleavage of the parent ion, which would produce the *t*-butoxy radical; however, calculations at the B3LYP/6-311++G(d,p) level suggest a more complex mechanism. The methyl-loss product can be viewed as an adduct of *t*-butoxy and acetone groups, $C_4H_9O{-}OC(CH_3)_2^+$, which is metastable with respect to dissociation to acetone and $C_4H_9O^+$. Modeling of the breakdown diagram suggests that this $C_4H_9O^+$ is a product of the sequential dissociation of the acetone-*t*-butoxy ion complex rather than the simple O−O

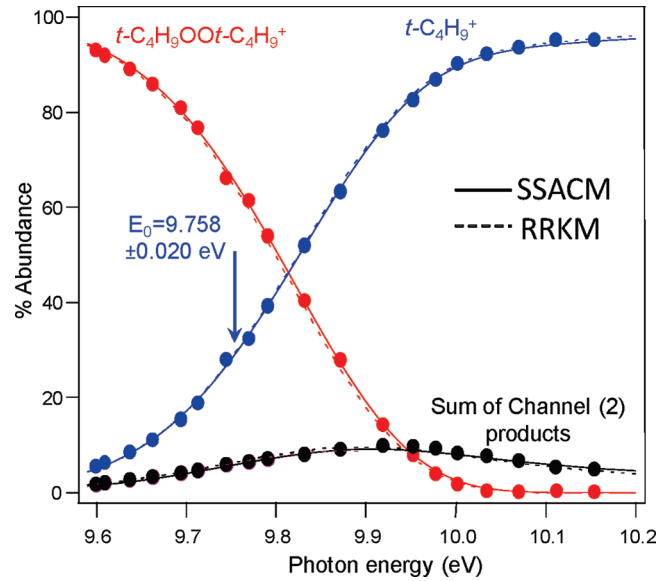

Figure 2. Breakdown diagram of di-*t*-butyl-peroxide. Circles are experimentally determined abundances, curves are best-fit simulations (see text). The sum of all products from Channel (2) are shown together (black circles and line).

bond break. We suggest, therefore, that the pathways for the dissociation of the di-*t*-butyl peroxide ion are as follows:

$$(CH_3)_3COOC(CH_3)_3^+ \rightarrow CH_3^\bullet + (CH_3)_2COOC(CH_3)_3^+ \quad (2a)$$

$$(CH_3)_2COOC(CH_3)_3^+ \rightarrow (CH_3)_2CO + C_4H_9O^+ \quad (2b)$$

$$(CH_3)_3COOC(CH_3)_3^+ \rightarrow (CH_3)_3COO^\bullet + C_4H_9^+ \quad (3)$$

Reactions 2 and 3 are in parallel, and reaction 2b is a sequential loss of acetone from the product of reaction 2a. Finally, calculations at the B3LYP/6-311++G(d,p) level suggest that the simple bond cleavage product ion of the sequential dissociation, *t*-$C_4H_9O^+$, is unstable and will isomerize to another structure, such as $CH_3OC(CH_3)_2^+$. This is in agreement with prior investigations of the $C_3H_7O^+$ species, which suggest several stable isomers including $HOC(CH_3)_2^+$, but not the isopropoxy ion.[36]

Modeling the Di-t-butyl Peroxide Ion Dissociation. The breakdown diagram in Figure 2 shows the fractional abundance of all ions as a function of the photon energy. The slow crossover for parent and fragment ions is a result of the di-*t*-butyl peroxide thermal energy distribution ($\langle E_{th} \rangle \approx 0.4$ eV) in the ion source and the slow (and varying) rate constant for dissociation. As the photon energy is increased, an ever greater percentage of ions have sufficient energy to dissociate. Once the photon energy is equal to or greater than E_0, all ions have sufficient energy to dissociate, however many of them may not have sufficient time to dissociate before being detected and will still be observed as parent di-*t*-butyl peroxide ions. In this case, only at photon energies well above threshold is the dissociation rate sufficiently high for all ions to dissociate on the time scale of the experiment. This causes the breakdown diagram to be instrument dependent in that the cross over energy (9.81 eV in Figure 2) can be shifted to lower energy by storing the ions

longer in the ionization region to permit them to dissociate. However, a practical limit is imposed by infrared radiative decay,[37] which stabilizes the parent ions at times longer than 0.01 s. As a result, the only way to extract the dissociation limit is to measure the decay rate constants over as large an ion energy range as possible and to use unimolecular rate theory to extrapolate from the experimentally measured region down to threshold.

The rate of the dissociation, $k(E)$, may be calculated using RRKM theory as a function of the internal energy of the ion by

$$k(h\upsilon + E_{th} - \mathrm{IE}) = \frac{\sigma N^{\dagger}(h\upsilon + E_{th} - E_0)}{h\rho(h\upsilon + E_{th} - \mathrm{IE})} \qquad (4)$$

where σ is the symmetry factor of the dissociation, $N^{\dagger}$ is the sum of states of the transition state, $h\upsilon$ is the photon energy, E_{th} is the thermal energy of the ion, IE is the adiabatic ionization energy of the neutral, h is Planck's constant, and ρ is the density of states of the dissociating ion. Reactions 2a and 3 appear to be simple bond cleavages, likely without any significant rearrangement of the dissociating molecule. As a result, the potential along the reaction coordinate will rise smoothly to the dissociated asymptote without ever passing through a maximum. With no energetic maximum, the location of the transition state is unclear, but can be defined by an entropic minimum along the reaction coordinate.[23] The location of this minimum is a function of the ion internal energy.

As previously stated, RRKM has not been very successful in modeling the dissociation rate curves of several ionic dissociations with large kinetic shifts.[21,27] Nonetheless, we employ RRKM here along with SSACM in order to further compare the efficacies of the two rate theories. A thorough description of using RRKM to determine E_0 in TPEPICO experiments can be found elsewhere.[38]

The starting point for the SSACM model assumes that the dissociation rate at energies close to the dissociation limit, where the transition state is at infinite product separation, will follow the orbiting transition state phase space theory (PST).[39–41] However, as the ion internal energy increases, the transition state moves closer in and any anisotropy of the potential along the reaction coordinate reduces the rate from that predicted by PST. SSACM accounts for anisotropy along the reaction coordinate by scaling the PST number of states of the orbital motion of the fragments by a "rigidity factor." In the language of eq 4, SSACM is employed by

$$N^{\dagger}(E) = \rho_{\mathrm{conserved}}(E)*[N^{\dagger}_{\mathrm{PST}}(E)f_{\mathrm{rigid}}(E)] \qquad (5)$$

where $N^{\dagger}_{\mathrm{PST}}$ is the PST number of states of the orbital motion of the products, $\rho_{\mathrm{conserved}}$ is the density of states of the conserved modes, f_{rigid} is a rigidity factor, and * indicates a convolution.

Troe has derived analytical forms for energy dependent f_{rigid} for several simple characteristic potentials.[26,42] Here we employ the form

$$f_{\mathrm{rigid}}(E) = \mathrm{e}^{-(E-E_0)/c} \qquad (6)$$

where c is treated as an optimizable parameter, but should show an increasing trend with the polarizability of the leaving neutral fragment. Note that like the RRKM analysis of the dissociation, SSACM has only two adjustable parameters, c and E_0, for each channel.

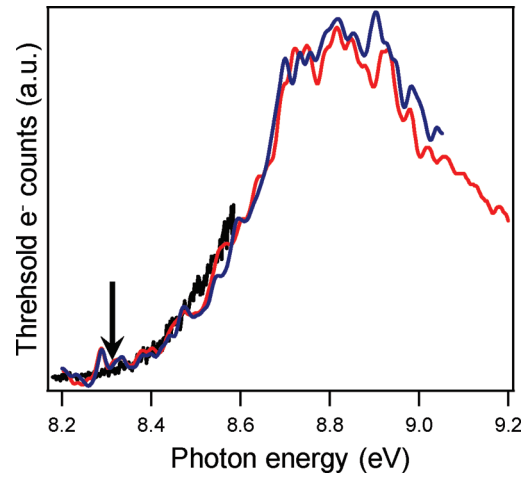

Figure 3. Threshold photoelectron spectrum of di-*t*-butyl peroxide at room temperature (red) and 235 K (blue) taken with the Chapel Hill TPEPICO apparatus, and at room temperature taken with the iPEPICO apparatus (black). Arrow indicates the adiabatic ionization potential calculated by the G3B3 method.

Both $\rho(E)$ and $N^{\dagger}(E)$ are calculated by the Beyer−Swinehart direct count method using the harmonic approximation for all modes, including those that are internal rotations. Treating internal rotations as Pitzer rotors would be more appropriate; however in this case, even at the highest excess energy sampled (~2 eV in the di-*t*-butyl peroxide ion) the low energy modes have ~5 kJ mol^{-1} on average, well below the barrier to methyl rotation. The true $\rho(E)$ should be well-approximated by the harmonic assumption and, in any case, moderate underestimation of $\rho(E)$ is accounted for by optimization to a higher value of the c fit parameter.

We have previously described the methods for analyzing parallel and sequential ionic dissociations using RRKM by simultaneously optimizing simulations of the breakdown diagram and TOF spectra.[38] The method here is identical with the exception of employing SSACM in place of RRKM for channels 2a and 3 (The rate of channel 2b, involving a rearrangement and a reverse barrier is modeled by RRKM).

The analysis depends on the accuracy of the adiabatic ionization energy (IE) of di-*t*-butyl peroxide to determine the ion internal energy distribution based on the photon energy. Although Batich and Adam[43] measured the photoelectron spectrum of di-*t*-butyl peroxide, the spectrum is broad and vibrationally unresolved, making determination of an adiabatic ionization energy difficult. It is unclear whether the slowly rising PES at low energies is a result of hot bands, which would suggest an IE close to the reported vertical IE of 8.78 eV, or if it is due to low ionization efficiency near the IE due to poor Franck−Condon overlap, suggesting an IE below 8.5 eV. To resolve this issue, we recorded threshold photoelectron spectra (TPES) at varying temperatures following a methodology described elsewhere.[44] Figure 3 shows TPES recorded at room temperature (295 K) and at 235 K. The spectra appear identical, suggesting that the shallow leading edge is not a result of hot bands, and that the IE lies near the onset of the signal between 8.25 and 8.4 eV. Calculations at the G3B3 level of (*t*-C_4H_9)OO(*t*-C_4H_9) and (*t*-C_4H_9)OO(*t*-C_4H_9)$^+$ yield an IE of 8.32 eV, in excellent agreement with our experimental spectra and we rely on this value for our analysis. An additional TPES taken

TABLE 1: Di-*t*-butyl Peroxide Ion Dissociation Best-Fit Rate Parameters (See Text) and E_0

		SSACM analysis		RRKM analysis	
channel	daughter ion	E_0 (eV)	c (cm^{-1})	E_0 (eV)	ΔS_{600K} (J mol^{-1} K^{-1})
2a	$(t\text{-}C_4H_9)OOC(CH_3)_2^+$	9.578 ± 0.040	38	9.448	16
3	$t\text{-}C_4H_9^+$	9.758 ± 0.020	228	9.671	60

using the iPEPICO setup, without temperature control of the sample temperature, but at a significantly higher photon resolution than the Chapel Hill setup and lower noise due to constant photon intensity as a function of wavelength, is also in excellent agreement.

The best-fit simulated breakdown diagram and TOF spectra are shown in Figures 1 and 2. The best-fit parameters for each channel are shown in Table 1. The uncertainties in the onsets are determined by the highest and lowest onsets for which no acceptable fit to the experimental data are possible. Examples of these limiting fits for the onset to channel (3) are shown in the insets of Figure 1. Limiting fits to the breakdown diagram are essentially coincident with the best-fit curve as the breakdown diagram may be reproduced with a wide range of onsets by compensating with faster or slower dissociation rates. In other words, the additional rate information contained in the TOF spectra is vital to accurately determining the onsets. It is important to note that despite significantly different best-fit values of E_0, both the RRKM and SSACM analyses fit the data throughout the experimentally measured range (Figures 1 and 2). That is, the fit to the data does not provide any clues about the appropriateness of the rate theory to extrapolate to the correct dissociation onset.

The best-fit rate curves calculated using SSACM and RRKM are compared in Figure 4. While the curves are nearly coincident over the range for which we can directly measure dissociation rates ($\sim 10^3 < k < 10^7$ s^{-1}), the curves deviate outside of, and in particular below, that range. That the rate curves deviate from one another by so much over an apparently small extrapolation suggests that any rate extrapolation must be done with great care, and that in order to obtain an accurate E_0 it is imperative to directly measure the rates at as low an energy as possible.

Table 1 also shows the best-fit E_0 determined by extrapolating near-threshold dissociation rates with RRKM. As seen in other studies of compounds with large kinetic shift,[21,27] RRKM significantly underestimates E_0 relative to SSACM. While RRKM is often inappropriate for modeling slow, barrierless ionic dissociations, there is no fundamental reason to believe that SSACM is appropriate in all such cases. SSACM results have been corroborated by either comparison to full SACM/CT treatments or to known dissociation onsets in only a handful of compounds, all of which are $C_6H_5X^+$ (X = H, *n*-C_4H_9, Cl, Br, I). As such, the analysis and derived onsets should be viewed with an appropriately skeptical eye and evaluated in the light of future evidence of SSACM's efficacy.

II. Di-*t*-butyl Diazene. The Mayer group recently reported TPEPICO measurements of di-*t*-butyl-diazene.[16] Here we report equivalent measurements that are in excellent agreement with the Mayer data; however, our analysis differs in several key respects. Most importantly, we note that the parent ion dissociates with almost no kinetic shift, and as a result the 0 K onsets from which thermochemical data may be derived are significantly higher than those previously reported.

The measured breakdown diagram of di-*t*-butyl diazene appears in Figure 5. The SLS data shown were collected using an 80 V cm^{-1} extraction field, which better separates the mass 56 and mass 57 peaks in the TOF spectra (Figure 6). Measurements were repeated in Chapel Hill at several photon energies using a 20 V cm^{-1} field and were in excellent agreement with the SLS data.

$(t\text{-}C_4H_9)NN(t\text{-}C_4H_9)^+$ dissociates through three parallel channels:

$$(t\text{-}C_4H_9)NN(t\text{-}C_4H_9)^+ \rightarrow C_4H_8^+ + (t\text{-}C_4H_9)NNH \quad (7)$$

$$\rightarrow (t\text{-}C_4H_9)NN^+ + t - C_4H_9^{\bullet} \quad (8)$$

$$\rightarrow t\text{-}C_4H_9^+ + (t\text{-}C_4H_9)\cdots NN^{\bullet} \quad (9)$$

Although both $(t\text{-}C_4H_9)OO(t\text{-}C_4H_9)^+$ and $(t\text{-}C_4H_9)NN(t\text{-}C_4H_9)^+$ dissociate to produce $t\text{-}C_4H_9^+$ as the primary product,

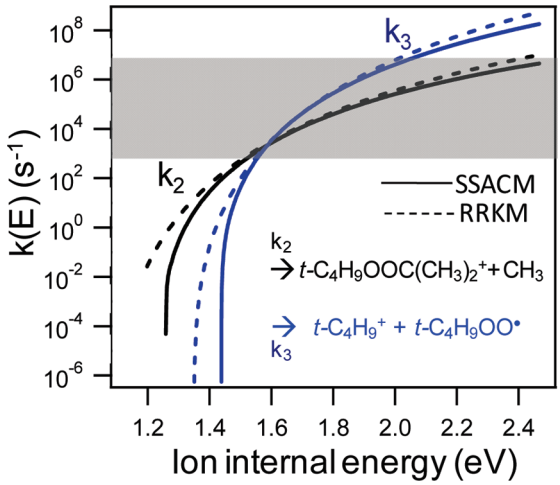

Figure 4. Best fit rate curves determined by SSACM (solid lines) and RAC-RRKM (dashed lines) rate theories for dissociation channels (2) and (3) (see text) of di-*t*-butyl peroxide ions. Shaded area indicates experimental window of directly measurable rates.

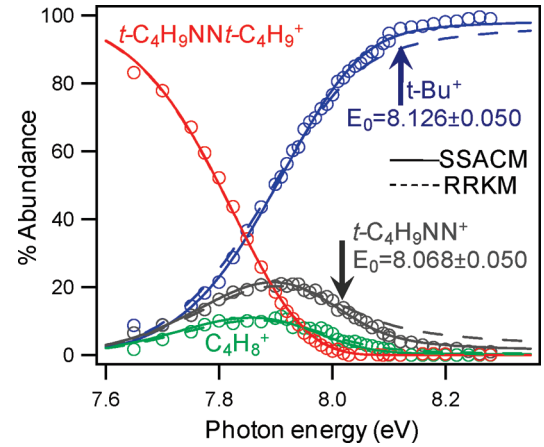

Figure 5. Breakdown diagram of di-*t*-butyl diazene ions collected with the iPEPICO setup at room temperature. Circles are experimental abundances; lines are best-fit simulations using either SSACM or RRKM rate theories (see text).

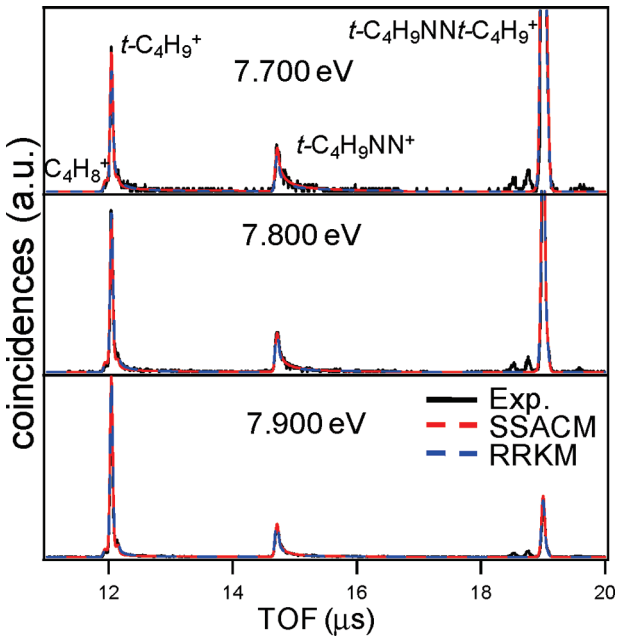

Figure 6. Experimental (black) and simulated (SSACM red, RRKM blue; nearly coincident) iPEPICO TOF distributions for di-*t*-butyl diazene ions at the indicated photon energies.

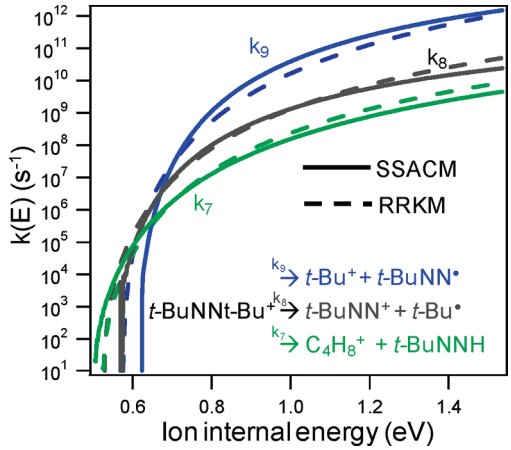

Figure 7. Best-fit rate curves of di-t-butyl-diazene ion dissociations determined using RRKM or SSACM rate theories (see text).

the dissociation pathways of the two species are quite different. Channel (7) has the lowest onset energy, and requires a rearrangement in order to form the isobutene ion. As such, it likely proceeds over a reverse barrier, and the data show it to occur at a much slower rate than the simple bond cleavage channels, which quickly grow in to dominate the reaction. Due to the reverse barrier, no thermochemical data can be derived from the onset to channel (7). Although we cannot entirely resolve the minor metastable mass 56 peak of channel (7) and the mass 57 peak of channel (9), it appears that channel (9) occurs fast on the time scale of our experiment, while both channels (7) and (8) appear as metastables.

Channels (8) and (9) both cleave the same C−N bond, with channel (8) placing the charge on the $C_4H_9NN^+$ species, and channel (9) placing the charge on the *t*-butyl. As we will show below by comparison of the experimental E_0 values of these channels and calculated energetics, the coproduct in channel (9) is a loosely bound adduct between the *t*-butyl radical and the N_2 molecule, whose calculated energy is close to the energy of the fully dissociated products of *t*-butyl radical + N_2 + *t*-butyl ion. In other words, the reaction does not appear to pass through

TABLE 2: Di-t-butyl Diazene Ion Dissociation Best-Fit E_0

		SSACM analysis		RRKM analysis	
channel	daughter ion	E_0 (eV)	c (cm^{-1})	E_0 (eV)	ΔS_{600K} (J mol^{-1} K^{-1})
7	$C_4H_8^+$	8.002[a]		8.023	−9
8	$(t\text{-}C_4H_9)NN^+$	8.069 ± 0.050	4.1	8.027	60
9	$t\text{-}C_4H_9^+$	8.122 ± 0.050	2.9	8.074	25

[a] The rate of channel 7 is modeled using RRKM.

a stable structure of the *t*-butyl diazyl radical, although a bound excited state structure was calculated (see Thermochemistry section). On the other hand, we will show that the *t*-butyl diazyl ion produced by channel (8) is stable so that the enthalpy of formation of this ion may be derived from the onset to this channel.

Fits were carried out for the 80 and 20 V cm^{-1} data using both RRKM and SSACM rate theories. In order to properly model metastable dissociation rates, an accurate adiabatic ionization energy of the di-*t*-butyl-diazene neutral is needed. Mayer et al. report an experimental IE of 7.55 eV determined by threshold photoelectron spectroscopy and a G3 calculated value of 7.4 eV.[16] In order to account for the uncertainty in the IE, the data were modeled at a range of values between 7.4 and 7.7 eV. The best fits were found by assuming an IE of 7.5 eV, and the variation in E_0 with different IE values is incorporated into the reported E_0 uncertainties.

The best-fit onsets to the 20 and 80 V cm^{-1} data were essentially identical. Modeled breakdown diagrams (Figure 5) and TOF spectra (Figure 6) show that both rate theories (RRKM and SSACM) provide good fits to the data. However, as in the case of the peroxide data, the derived onsets depended on whether SSACM or RRKM was used to model the data (Table 2). In the analysis, we assume that the rate constant for reaction 7 is properly modeled by RRKM theory because it is a tight transition state. The derived RRKM and SSACM onsets for reaction 8 differ by 40 meV. For reaction 9 this difference increases to 50 meV. Because the competition of these reactions with the lowest energy channel moves the observed signals to higher energies, they require a larger extrapolation to the onset. As in the case of the peroxide data, we accept the SSACM onsets as more reliable. The SSACM-derived onsets for channels (8) and (9), 8.068 ± 0.050 and 8.126 ± 0.050 eV, respectively, are 0.238 and 0.186 eV higher than those reported by Mayer et al.[16]

As in the di-*t*-butyl peroxide ion dissociation, we are unable to distinguish between the RRKM and SSACM modeled fits. Although the RRKM fits also diverge from the measured abundances at higher photon energies, it is not apparent that this is a failure of the modeling. Based on the measured onset for channel (8), the *t*-butyl diazyl ion is just 14 kJ mol^{-1} more stable than the dissociated products $t\text{-}C_4H_9^+$ and N_2. Thus, *t*-butyl diazyl ions with even moderate internal excitation will dissociate to $t\text{-}C_4H_9^+$. Because the product ion of the sequential dissociation is the same as that produced directly by channel (9), the $t\text{-}C_4H_9^+$ experimental abundance may be elevated over that calculated without assuming sequential dissociation.

Unlike the di-*t*-butyl peroxide ion dissociation (see below), the RRKM and SSACM onsets are too close together in energy to distinguish between them by ab initio thermochemistry. Because channels (8) and (9) differ by which fragment retains the charge, their onsets should differ by the ionization energies of the two fragments. Calculations using various model chemistries reproduce the known IE of $t\text{-}C_4H_9$ and suggest that the

onset to (8) should be lower than the onset to (9) by 81 meV (G2), 106 meV (G3B3), and 86 meV (CBS-APNO). This is in reasonable agreement with the SSACM-derived onsets, which differ by 60 meV, while the RRKM-derived onsets differ by 45 meV. Additionally, Mayer reports G3 calculated endothermicities of $(t\text{-}C_4H_9)NN(t\text{-}C_4H_9)^+ \rightarrow (t\text{-}C_4H_9)NN^+ + t\text{-}C_4H_9$ and $(t\text{-}C_4H_9)NN(t\text{-}C_4H_9)^+ \rightarrow (t\text{-}C_4H_9)NN + t\text{-}C_4H_9^+$ to be 52 and 62 kJ mol^{-1}, respectively, suggesting E_0 for channels (8) and (9) to be 8.04 and 8.14 eV. Although the G3 values are in excellent agreement with the SSACM-derived onsets, the uncertainty of the calculations (on the order of 10 kJ mol^{-1}) does not rule out the RRKM-derived values.

Thermochemistry. The derived *t*-butyl peroxy radical heat of formation depends on the heats of formation of di-*t*-butyl peroxide and $t\text{-}C_4H_9^+$, and the thermochemistry of those two compounds are briefly reviewed here. The heat of formation of di-*t*-butyl peroxide has been of interest because of its use as an initiator in photoacoustic calorimetry experiments. The gas phase heat of formation has been established by determination of the liquid phase heat of formation by combustion calorimetry[45,46] and of the enthalpy of vaporization by varying methods.[45] There is little variation in reported values of the heat of combustion, but the reported enthalpy of vaporization ranges from 31.0 to 40.1 kJ mol^{-1}. Here we rely on the most recent and careful determination of both the heat of combustion and vaporization by Diogo et al.,[45] yielding a gas phase heat of formation of -341.5 ± 2.2 kJ mol^{-1}, a value accepted by the photoacoustic calorimetry community.[47] We note that the most recent compilation of thermochemical data by Pedley[48] predates the Diogo et al. measurements and reports a significantly different heat of formation based on a much lower value of the enthalpy of vaporization. Additionally, although the NIST webbook database suggests a slightly different value of the di-*t*-butyl peroxide heat of formation by rejecting the recent enthalpy of vaporization measurement in favor of a slightly higher value determined in 1951, we see no justification for using the older value.

Two stable ionic $C_4H_9^+$ structures have been identified: the *s*-butyl ion and the branched *t*-butyl ion,[49] the latter being more stable and the obvious product in the dissociation of the di-*t*-butyl peroxide. The heat of formation of the *t*-butyl ion has recently been determined by our group by TPEPICO spectroscopy of neopentane. The 0 K value of 737.1 ± 2.5 kJ mol^{-1} is in good agreement with previous measurements,[50,51] but has more appropriately assigned uncertainty.

The 0 K heat of formation of the $(t\text{-}C_4H_9)OO^\bullet$ radical is determined by (1) along with the 0 K heat of formation of $t\text{-}C_4H_9^+$ and $(t\text{-}C_4H_9)OO(t\text{-}C_4H_9)$. The latter is calculated by applying a thermal correction to the known 298 K heat of formation by the standard thermochemical cycle. Several of the normal modes in di-*t*-butyl peroxide are internal rotations, for which the harmonic approximation may be poor. McClurg et al.[52] derived an analytical approximation to the hindered rotor density of states (later corrected by Knyazev[53]) with which they report an analytical correction to account for deviation of internal rotations from harmonic behavior. Barriers to rotation for the coupled internal modes were determined by a series of constrained optimizations at the B3LYP/6-311++G(d,p) level mimicking the calculated normal modes. The barriers were sufficiently high (>30 kJ mol^{-1}) that the sum of the corrections is negligible (~0.1 kJ mol^{-1}) The $H_{298K} - H_{0K}$ thermal correction and the 0 K heats of formation of di-*t*-butyl peroxide and *t*-butyl peroxy radical are shown in Table 3.

The 298 K heat of formation of *t*-butyl peroxy radical, -109.7 ± 3.9 kJ mol^{-1}, is determined from the 0 K heat of formation by applying a similar thermal correction including corrections for internal rotation. This is the most precise experimental determination of the heat of formation of the *t*-butyl peroxy radical that we are aware of. Blanksby et al. report a bond dissociation energy of *t*-butyl hydrogen peroxide, from which they derive a *t*-butyl peroxy radical heat of formation of -105.4 ± 10.5 kJ mol^{-1}.[3] However, if a more recent determination of the *t*-butyl hydrogen peroxide[18] heat of formation is used as an anchor, the radical heat of formation is adjusted to -99.6 kJ mol^{-1}, at the edge of reasonable agreement with the current value. Both experimental values are in reasonable agreement with the value of -103.3 kJ mol^{-1} calculated by isodesmic reactions using the high level CBS-QB3 and CBS-APNO ab initio methods, but the reported sub-kJ accuracy in the calculated value appears to be exceptionally optimistic.[5] Less-reliable calculated values by the G3 method (without employing isodesmic calculations), -103.2 kJ mol^{-1},[8] and by lower-level calculations and group additivity, -105.4 kJ mol^{-1},[6] are also in acceptable agreement with our value.

TABLE 3: Derived and Ancillary Thermochemical Data (kJ mol^{-1})

	$\Delta H^\circ_{f,0K}$	H_{298-0K}	$\Delta H^\circ_{f,298K}$
$(t\text{-}C_4H_9)OO(t\text{-}C_4H_9)$	−285.9	37.7	-341.5 ± 2.2[a]
$t\text{-}C_4H_9$	74.9	19.2	51.8 ± 2[b]
$t\text{-}C_4H_9^+$	737.1	19.0	714.3 ± 2.5[c]
$(t\text{-}C_4H_9)OO^\bullet$	−81.1	22.4	-109.7 ± 3.9[d]
$(t\text{-}C_4H_9)NN(t\text{-}C_4H_9)$	20.0	36.9	-36.4 ± 2.8[e]
$t\text{-}C_4H_9NN^+$	723.6	28.5	701.2 ± 5.9[d]
$t\text{-}C_4H_9NN^\bullet$[f]	66.5±6.1		

[a] Diogo et al. [45] [b] Berkowitz et al. [17] [c] Stevens et al.[18] [d] This work. [e] Montgomery et al.[54] [f] May be a bound species at 0 K, but not at 298 K; see text.

The experimentally derived heat of formation using the onset determined with RRKM is -119.2 ± 4 kJ mol^{-1}, well outside of mutual uncertainty with the SSACM derived result, the previous experimental value, and the calculated values. We suggest that the better agreement of the SSACM value provides further evidence that SSACM correctly extrapolates the rates barrierless ionic dissociations down to threshold, whereas RRKM overestimates the kinetic shift in such systems.

Along with the previously determined di-*t*-butyl peroxide and *t*-butyl radical heats of formation, the *t*-butyl peroxy radical heat of formation defines the C−O bond dissociation enthalpy (BDE) of neutral di-*t*-butyl peroxide to be 283.8 ± 4.1 kJ mol^{-1}. This number is in contrast to the previously reported value of 295.8 ± 8.4 kJ mol^{-1} derived by Luo.[12]

Thermochemical data can also be derived from the di-*t*-butyl diazene onsets by anchoring onto the neutral heat of formation and the *t*-butyl radical and ion heats of formation. Engel and co-workers determined the di-*t*-butyl diazene gas phase heat of formation through several calorimetry experiments and report an evaluated 298 K value of -36.4 ± 2.8 kJ mol^{-1}.[54] The heats of formation of *t*-butyl radical and ion are discussed above. However, the TPEPICO experiment gives no direct information about the identity of the neutral coproduct(s) of a dissociation. In order to extract thermochemical data from the measured E_0 values, the coproducts must be identified, so that an appropriate heat of formation may be assigned. The identification can often be made by employing high level calculations to approximate the energetics of possible product channels.

If we assume a simple bond cleavage for channel (8), the expected products are *t*-butyl diazyl ion and *t*-butyl radical. If this is the case, the measured E_0 implies a heat of formation of

t-butyl diazyl ion of $\Delta H^{\circ}_{f,0K} = 723.6 \pm 6$ kJ mol^{-1} and 0 K C−N BDE of 13 kJ mol^{-1}. Calculations using the G3B3 model chemistry suggest an identical BDE of 13.0 kJ mol^{-1}, and we can safely assume that the channel produces *t*-butyl radical and a weakly bound ion structure with C_3 symmetry.

Making a similar assumption for channel (9), the expected products are *t*-butyl diazyl radical and the *t*-butyl ion. Because the *t*-butyl ion heat of formation is well-known, the measured E_0 implies a heat of formation of *t*-butyl diazyl radical of $\Delta H^{\circ}_{f,0K} = 66.5 \pm 6.1$ kJ mol^{-1} and a 0 K C−N BDE of only 8.4 ± 6.5 kJ mol^{-1}. A structure that corresponds to such a weakly bound species, and one that seems to be a stationary point on the B3LYP/6-311++G(d,p) potential energy surface, was found by assuming an elongated C−N bond. However, we note that at this level of theory, three low-energy internal modes are described by imaginary frequencies, which may indicate that this is not a proper minimum energy structure. It is also possible that these small imaginary frequencies, taken along with the vanishingly small forces calculated at this geometry, may be indicative of the inability of DFT to describe van der Waals interactions reliably. The calculated 0 K BDE of this structure is 2.8 kJ mol^{-1}, which is in good agreement with the experimental value. Such a small binding energy, which is considerably smaller than the 298 K thermal energy of about 25 kJ mol^{-1}, means that this species is essentially unbound, which is a conclusion that was also reached by the Mayer group.[16]

It is interesting to compare the *t*-butyl diazyl radical and ionic structures and energetics. They both have very long C−N bonds and are weakly bound, the former by a few kJ mol^{-1} and the latter by 13 kJ mol^{-1}. The ionic structure is certainly stable because it is observed in the TOF spectra. However, we have no way of knowing how long the neutral radical structure remains together. In both cases, though, the bonding seems to be of a van der Waals type, with the stronger ionic bond being aided by ion induced dipole forces.

It is worth reporting that we found a higher energy structure for the *t*-C_4H_9NN radical that lies 79 kJ mol^{-1} above its dissociation limit using the G3B3 model chemistry. Unlike the lower energy structure, its C−N bond distance was more in line with a covalent bond and is clearly a minimum in the PE surface. The calculated energies of the methyl, ethyl, and isopropyl analogues of this structure agree well with the reported heats of formation for those radicals determined by the rate of decomposition of neutral dialkyl diazenes.[11]

Summary

The *t*-butyl peroxy radical heat of formation has been determined by measuring the ionic dissociation onset of di-*t*-butyl peroxy by TPEPICO spectroscopy. A simplified version of the statistical adiabatic channel model was used to extrapolate the dissociation rate from measured values at higher ion internal energies down to the dissociation threshold. The reasonable agreement between the 298 K heat of formation of -109.7 ± 3.9 kJ mol^{-1} with previous values lends further support to the efficacy of the SSACM.

The *t*-butyl diazyl ion heat of formation has been determined by iPEPICO spectroscopy of di-*t*-butyl diazene, while the *t*-butyl diazyl radical is shown to be an essentially unbound species. The experimental values were in good agreement with high-level ab initio calculations.

In both systems, E_0 values determined using RRKM were significantly lower than those determined using SSACM. The di-*t*-butyl peroxide ion dissociation occurs with a large kinetic shift, and previous work has shown that, as a result, RRKM will likely overestimate that shift. The di-*t*-butyl diazene ion dissociation occurs with only a small kinetic shift; however, this work presents evidence that RRKM may also overestimate the competitive shift in a parallel, barrierless ionic dissociation.

Acknowledgment. We thank the U.S. Department of Energy (DOE Grant DE-FG02-97ER14776), the US National Science Foundation, and the Swiss Federal Office of Energy (BFE contract 101969/152433) for financial support of this work. We also thank Will Stevens for valuable discussions and for providing us with the *t*-butyl ion heat of formation.

Supporting Information Available: Calculated neutral and ion harmonic frequencies are provided. This material is available free of charge via the Internet at http://pubs.acs.org.

References and Notes

(1) Frost, G. J.; Ellison, G. B.; Vaida, V. *J. Phys. Chem. A* **1999**, *103* (49), 10169–10178.
(2) Goldstein, S.; Samuni, A.; Hideg, K.; Merenyi, G. *J. Phys. Chem. A* **2006**, *110* (10), 3679–3685.
(3) Blanksby, S. J.; Ramond, T. M.; Davico, G. E.; Nimlos, M. R.; Kato, S.; Bierbaum, V. M.; Lineberger, W. C.; Ellison, G. B.; Okumura, M. *J. Am. Chem. Soc.* **2001**, *123* (39), 9585–9596.
(4) Meloni, G.; Zou, P.; Klippenstein, S. J.; Ahmed, M.; Leone, S. R.; Taatjes, C. A.; Osborn, D. L. *J. Am. Chem. Soc.* **2006**, *128* (41), 13559–13567.
(5) Simmie, J. M.; Black, G.; Curran, H. J.; Hinde, J. P. *J. Phys. Chem. A* **2008**, *112* (22), 5010–5016.
(6) Lay, T. H.; Bozzelli, J. W. *J. Phys. Chem. A* **1997**, *101* (49), 9505–9510.
(7) Sebbar, N.; Bozzelli, J. W.; Bockhorn, H. *J. Phys. Chem. A* **2004**, *108* (40), 8353–8366.
(8) Janoschek, R.; Rossi, M. J. *Int. J. Chem. Kin.* **2004**, *36* (12), 661–686.
(9) Zhu, L.; Bozzelli, J. W.; Kardos, L. M. *J. Phys. Chem. A* **2007**, *111* (28), 6361–6377.
(10) Engel, P. S. *Chem. Rev.* **1980**, *80* (2), 99–150.
(11) Acs, G.; Peter, A. *Int. J. Chem. Kin.* **1987**, *19* (10), 929–942.
(12) Luo, Y.-R. *Comprehensive Handbook of Chemical Bond Energies*; CRC Press: Boca Raton, FL, 2007.
(13) Ramsperger, H. C. *J. Am. Chem. Soc.* **1927**, *49*, 912–916.
(14) Diau, E. W. G.; Zewail, A. H. *ChemPhysChem* **2003**, *4* (5), 445–456.
(15) Holmes, J. L.; Lossing, F. P.; Mayer, P. M. *J. Am. Chem. Soc.* **1991**, *113*, 9723–9728.
(16) Rabaev, M.; Boulanger, A. M.; Holland, D. M. P.; Shaw, D. A.; Mayer, P. M. *J. Phys. Chem. A* **2009**, *113* (8), 1518–1522.
(17) Berkowitz, J.; Ellison, G. B.; Gutman, D. *J. Phys. Chem.* **1994**, *98*, 2744–2765.
(18) Stevens, W. R.; Walker, S. H.; Shuman, N. S.; Baer, T. *J. Phys. Chem. A*, DOI: 10.1021/jp908583j.
(19) Chupka, W. A. *J. Chem. Phys.* **1959**, *30*, 191–211.
(20) Baer, T.; Hase, W. L. *Unimolecular Reaction Dynamics: Theory and Experiments*; Oxford University Press: New York, 1996.
(21) Stevens, W.; Sztáray, B.; Shuman, N.; Baer, T.; Troe, J. *J. Phys. Chem. A* **2009**, *113*, 573–582.
(22) Chesnavich, W. J. *J. Chem. Phys.* **1986**, *84*, 2615–2619.
(23) Hase, W. L. *J. Chem. Phys.* **1976**, *64*, 2442–2449.
(24) Klippenstein, S. J.; Marcus, R. A. *J. Chem. Phys.* **1989**, *91*, 2280–2292.
(25) Maergoiz, A. I.; Nikitin, E. E.; Troe, J.; Ushakov, V. G. *J. Chem. Phys.* **2002**, *117* (9), 4201–4213.
(26) Troe, J.; Ushakov, V. G.; Viggiano, A. A. *J. Res. Phys. Chem. Chem. Phys.* **2005**, *219* (5), 715–741.
(27) Troe, J.; Ushakov, V. G.; Viggiano, A. A. *J. Phys. Chem. A* **2006**, *110*, 1491–1499.
(28) Sztáray, B.; Baer, T. *Rev. Sci. Instrum.* **2003**, *74*, 3763–3768.
(29) Kercher, J. P.; Stevens, W.; Gengeliczki, Z.; Baer, T. *Int. J. Mass Spectrom.* **2007**, *267*, 159–166.
(30) Baer, T.; Li, Y. *Int. J. Mass Spectrom.* **2002**, *219*, 381–389.
(31) Bodi, A.; Johnson, M.; Gerber, T.; Gengeliczki, Z.; Sztáray, B.; Baer, T. *Rev. Sci. Instrum.* **2009**, *80*, 034101.
(32) Johnson, M.; Bodi, A.; Schulz, L.; Gerber, T. *Nucl. Instr. and Meth. in Phys. Res. A* **2009**, *610*, 597−603.
(33) Bodi, A.; Sztáray, B.; Baer, T.; Johnson, M.; Gerber, T. *Rev. Sci. Instrum.* **2007**, *78*, 084102.

(34) Frisch, M. J.; Trucks, G. W.; Schlegel, H. B.; Scuseria, G. E.; Robb, M. A.; Cheeseman, J. R.; Montgomery, J. A.; Vreven, T.; Kudin, K. N. ; Burant, J. C.; Millam, J. M.; Iyengar, S. S.; Tomasi, J.; Barone, V.; Mennucci, B.; Cossi, M.; Scalmani, G.; Rega, N.; Petersson, G. A.; Nakatsuji, H.; Hada, M.; Ehara, M.; Toyota, K.; Fukuda, R.; Hasegawa, J.; Ishida, M.; Nakajima, T.; Honda, Y.; Kitao, O.; Nakai, H.; Klene, M.; Li, X.; Knox, J. E.; Hratchian, H. P.; Cross, J. B.; Adamo, C.; Jaramillo, J.; Gomperts, R.; Stratmann, F.; Yazyev, O.; Austin, A. J.; Cammi, R.; Pomelli, C.; Ochterski, J. W.; Ayala, P. Y.; Morokuma, K.; Voth, G. A.; Salvador, P.; Dannenberg, J. J.; Zakrzewski, V. G.; Dapprich, S.; Daniels, A. D.; Strain, M. C.; Farkas, ö.; Malick, D. K.; Rabuck, A. D.; Raghavachari, K.; Foresman, J. B.; Ortiz, J. V.; Cui, Q.; Baboul, A. G.; Clifford, S.; Cioslowski, J.; Stefanov, B. B.; Liu, G.; Liashenko, A.; Piskorz, P.; Komáromi, I.; Martin, R. L.; Fox, D. J.; Keith, T.; Al-Laham, M. A.; Peng, C. Y.; Nanayakkara, A.; Challacombe, M.; Gill, P. M. W.; Johnson, B.; Chen, W.; Wong, M. W.; Gonzalez, C.; Pople, J. A. *Gaussian 03, Revision C.02*: Gaussian, Inc.: Wallingford, CT, 2004.

(35) Merrick, J. P.; Moran, D.; Radom, L. *J. Phys. Chem. A* **2007**, *111* (11683), 11683–11700.

(36) Holmes, J. L.; Aubry, C.; Mayer, P. M. *Assigning Structures to Ions in Mass Spectrometry*; CRC Press: Boca Raton, FL, 2007.

(37) Dunbar, R. C. *Mass Spectrom. Rev.* **1992**, *11*, 309–339.

(38) Baer, T.; Sztáray, B.; Kercher, J. P.; Lago, A. F.; Bodi, A.; Scull, C.; Palathinkal, D. *Phys. Chem. Chem. Phys.* **2005**, *7*, 1507–1513.

(39) Chesnavich, W. J.; Bowers, M. T. *J. Chem. Phys.* **1977**, *66*, 2306–2315.

(40) Klots, C. E. *J. Phys. Chem.* **1971**, *75*, 1526–1532.

(41) Pechukas, P.; Light, J. C. *J. Chem. Phys.* **1965**, *42*, 3281–3291.

(42) Troe, J. *J. Chem. Soc., Faraday Trans.* **1997**, *93* (5), 885–891.

(43) Batich, C.; Adam, W. *Tetrahedron Lett.* **1974**, (16), 1467–1470.

(44) Shuman, N. S.; Ochieng, M. A.; Sztáray, B.; Baer, T. *J. Phys. Chem. A* **2008**, *112* (25), 5647–5652.

(45) Diogo, H. P.; Minas da Piedade, M. E.; Martinho Simões, J. A.; Nagano, Y. *J. Chem. Thermodyn.* **1995**, *27* (6), 597–604.

(46) Baker, G.; Little, J.; Shaw, R.; Thynne, J. C. J. *J. Chem. Soc.* **1965**, (DEC), 6970.

(47) Laarhoven, L. J. J.; Mulder, P.; Wayner, D. D. M. *Acc. Chem. Res.* **1999**, *32* (4), 342–349.

(48) Pedley, J. B. *Thermochemical Data and Structures of Organic Compounds*; Thermodynamics Research Center: College Station, 1994.

(49) Oliveira, M. C.; Baer, T.; Olesik, S.; Almoster Ferreira, M. A. *Int. J. Mass Spectrom. Ion. Proc.* **1988**, *82*, 299–318.

(50) Keister, J. W.; Riley, J. S.; Baer, T. *J. Am. Chem. Soc.* **1993**, *115*, 12613–12614.

(51) Smith, B. J.; Radom, L. *J. Am. Chem. Soc.* **1993**, *115*, 4885–4888.

(52) McClurg, R. B.; Flagan, R. C.; Goddard, W. A. I. *J. Chem. Phys.* **1997**, *106* (16), 6675–6680.

(53) Knyazev, V. *J. Chem. Phys.* **1999**, *111* (15), 7161–7162.

(54) Montgomery, R. L.; Engel, P. S.; Leckonby, R. A.; Rossini, F. D.; Mansson, M.; Szilagyi, S.; Timberlake, J. W. *J. Chem. Eng. Data* **1978**, *23* (2), 129–131.

JP907767C